# Structure and Chemical Trends in Doped Silicon Nanocrystals

Zhiyong Zhou, Michael L Steigerwald, Richard A Friesner, and Louis Brus

Department of Chemistry, Columbia University, New York, NY 10027

Mark S Hybertsen

Department of Applied Physics and Applied Mathematics and Center for Electron Transport in Molecular Nanostructures, Columbia University, New York, NY 10027

Electronic and structural properties of substitutional group-V donors (N, P, As, Sb) and group-III acceptors (B, Al, Ga, In) in silicon nanocrystals with hydrogen passivation are explored using first principles calculations based on hybrid density functional theory with complete geometrical optimization. The bonding near the impurity is similar to that found for the impurity in bulk crystalline silicon, with some quantitative differences. The N case shows large local distortions, as it does in the bulk, characteristic of a deep trap. For the other impurities, no evidence is found for a transition to atomic scale localization induced by the small size of the nanocrystal. The chemical trends of the donor and acceptor binding energies and the donor excited state energies in doped nanocrystals are similar to those in the bulk; however, the absolute magnitudes are substantially larger. The increase in the magnitude of the binding energy is mainly due to the quantum confinement effect combined with the reduced screening of the impurity potential in small nanocrystals. The screening of the impurity potential is carefully examined using the self-consistent electrostatic potential from the full calculations. Strong chemical and local-field effects are seen within the radius of the first neighbor

bonds to the impurity atom. This explains the large increase in the donor excited state energy level splittings and the relative importance of the central cell contributions to the binding energies. The acceptor and donor orbitals have different atomic character on the impurity site leading to substantially different acceptor and donor energy level splittings.

73.22.-f, 71.55.Cn, 61.46.+w

## I. Introduction

Silicon nanocrystals are different than bulk silicon in several significant ways. The nanocrystal band gap increases with decreasing size down to about 3 nm diameter in passivated nanocrystals, as expected from a quantum size effect model[1]. Below about 3nm in size, oxide passivated nanocrystals luminesce at lower energy than hydrogen passivated nanocrystals[2]. Calculation shows that the size of the band gap, and the corresponding spatial pattern of the highest occupied molecular orbital (HOMO) and lowest unoccupied molecular orbital (LUMO), depend upon the electronegativity of the passivating layer at such small size[3,4]. In oxide-terminated nanocrystals the HOMO is drawn to the surface and resides in weakened Si-Si backbonds on interfacial Si atoms directly bonded to oxygen. The band gap is relatively independent of size below 3 nm with oxide passivation, in contrast to H terminated nanocrystals.

As first discovered in porous silicon[5], the 23 $^{o}$C Si nanocrystal luminescence quantum yield is very high compared with bulk Si. This is principally a kinetic effect, in that quantum confinement keeps the photoexcited electron and hole superimposed (unlike the bulk crystal) in one crystallite[6]. Such small nanocrystals remain essentially indirect

gap materials in which the phonon assisted radiative processes dominate over most of the observed size range[7]. In Si nanostructures there is also a major change in electrostatics, due to the presence of interfaces between high (silicon) and low (outside) dielectric constants.[8,9] Electric fields from electrons and holes fringe outside of the nanocrystals. This effect leads to size dependent charging (ie, ionization) energies, and to electron and hole kinetic relaxation rates that depend strongly upon the polarizability of matter outside the nanostructure[10].

Microscopic understanding of defects and impurities in silicon nanocrystals is still in an early stage. Nevertheless, recent proposals have been put forward to use the P electron spin near a gate electrode in a nanostructure as the physical basis for quantum computing[11]. In bulk semiconductors, the chemical trends in donor and acceptor energy levels proved to be a critical challenge for the simple hydrogenic Wannier model and stimulated a much deeper microscopic understanding of semiconductor physics[12]. In a similar way, many trends in the electronic and optical properties of semiconductor nanocrystals can be understood based on ideas from effective mass theory. However, given the dramatic impact of altered screening in semiconductor nanocrystals, and the possible occurrence of a sudden transition to atomic scale localization of the carrier, it is a fundamental question as to how localized the donor or acceptor wavefunctions will be. An intriguing recent paper[13] suggesting that the ionization potential of P-doped silicon nanocrystal is independent of size, highlights this possibility. In this work, we present a detailed study of group-V donors and group-III acceptors in Si nanocrystals based on ab initio calculations with complete geometrical optimization. Since controlled experiments

with doped nanocrystals are not yet possible, such atomic scale calculations provide the first view of this problem.

## II. Theoretical Methods

It is important to use methods that are known to quantitatively reproduce a diverse range of chemical bonding situations in finite structures with real surfaces. We use a real space, atom-centered basis and a hybrid functional in density functional theory (DFT) that combines exact Hartree-Fock exchange with the generalized gradient approximation. Invented a decade ago, hybrid functionals reproduce experimental bond energies and ionization potentials in a standard test set of small molecules with residual errors of 0.13 eV, about 10% of the residual errors found for the commonly used local density approximation (LDA).[14,15] More recently, it was found that hybrid functionals give an improved band structure and band gap for semiconductors such as crystalline Si in comparison to LDA[16]. The improvement for complex crystalline oxides such as $La_2CuO_4$, $CaCuO_2$, $LaMnO_3$, $Cr_2O_3$, NiO, $TiO_2$, and $UO_2$ is more dramatic; in these oxides LDA often gives qualitatively incorrect (metallic) results [16,17].

We use the B3LYP hybrid functional[14]. The static DFT calculations were performed on personal computers using the Jaguar 5.0 code[18]. Complete geometric optimization of species with up to about 200 atoms can be done. We do not assume any symmetry. Calculations were done with all electron 6-31g* basis for the Si, the passivating H and the first and second row impurities under study. Heavier impurities were studied using pseudopotentials with the LAV3P basis[19]. Spin orbit effects are not included in our calculations. In the case of the ionized species, we reoptimize structure in the presence (or absence) of the extra charge, in order to understand changes in the doped

nanocrystal geometry as a function of charge state. The vertical ionization potential is the total energy difference when the ion is converged for the fixed geometry of the neutral. The adiabatic ionization potential is the energy difference when the ion is also geometrically optimized. The difference between the vertical and adiabatic ionization potential is the hole Franck-Condon reorganization energy. Similarly, vertical and adiabatic electron affinities are calculated. The difference between them is the electron reorganization energy. The average of the ionization potential and electron affinity gives the chemical potential while the difference between them is the chemical hardness, corresponding to an effective charging energy.

## III. Results

### A. Donors

As previously reported[3], the optimized $Si_{35}H_{36}$ and $Si_{87}H_{76}$ nanocrystals in Figure 1 are $T_d$ symmetry with H terminated 111 surface facets. We study four different chemically doped Si nanocrystals with group-V elements: N, P, As and Sb. With P in the center position, there is little change in geometrical structure. The four $sp^3$ P-Si 2.41 Å bonds in the larger nanocrystal are just slightly expanded from the parent nanocrystal 2.38 Å Si-Si lengths. If the extra electron is removed, the reoptimized bond length contracts slightly to 2.38 Å. If an extra electron is added to form an electron pair in the P centered orbital, the P-Si bonds expand slightly to 2.45 Å. This $sp^3$ physical structure, relatively independent of charge state, is very similar to a substitutional P dopant in bulk Si[20,21]. In $Si_{86}AsH_{76}$ and $Si_{86}SbH_{76}$, the four central X-Si bond lengths are 2.51 Å and

2.64 Å, respectively. This exceeds the bond expansion calculated for substitutional As and Sb impurities in bulk crystalline Si by about 0.1 Å[20]. Similarly, if an extra electron is removed (added), the reoptimized bond length shortens (lengthens) slightly by 0.04 Å. Since N is a deep donor in bulk Si, it is perhaps not surprising that the local bonds around the N in the nanocrystal distort substantially. The symmetry of the nanocrystal is lowered to $C_{3v}$. In the neutral state, one bond is essentially broken (3.23 Å) while the remaining 3 N-Si bonds shorten to 1.87 Å and the Si-N-Si bond angles are close to 120 degrees. This is very similar to the relaxed bond length calculated for neutral substitutional N in bulk Si[22]. Ionization to form the cation nearly restores the local symmetry, but with short N-Si bonds (about 2.05 Å).

The electronic energy levels near the HOMO and LUMO for the undoped and doped nanocrystals are shown in Figure 2. In the parent undoped nanocrystal the LUMO is composed of three essentially accidentally degenerate orbitals – $A_1$, E and $T_2$. This result is consistent with previous calculations[23], which indicate that the symmetry of the HOMO is usually $T_2$ while the LUMO is $A_1$, E or $T_2$ depending on size. For larger size nanocrystals, the energies of those three types of orbitals are essentially degenerate. These groups of one $A_1$ state, one twofold-degenerate E state, and one threefold-degenerate $T_2$ state in our DFT calculation for the finite-size Si nanocrystal originate from the six degenerate conduction band minima along (100) and equivalent directions. The orbital shapes are illustrated in the Figure 3. The $A_1$ orbital is s-like, with a large component on center atom. The $T_2$ and E orbitals have a node on the center atom due to symmetry.

The impurity potential splits the $A_1$, $T_2$, and E states. For the electron-doped nanocrystals $Si_{86}XH_{76}$ or undoped nanocrystal anion $Si_{87}H_{76}^-$, the ground electronic state has a singly occupied $A_1$ orbital. For the P, As and Sb impurities, as seen in Figure 2, the empty $T_2$ and E orbitals are about 1 eV higher than the singly occupied $A_1$. For the N case there is a much larger splitting, consistent with the large change in geometry. By manually changing the occupation of the initial wavefunctions, convergence to two excited states is also obtained, corresponding to a singly occupied $T_2$ orbital and E orbital, respectively. The symmetry of these two optimized excited nanocrystals is lowered to $D_2$ from $T_d$. The total energy difference between these excited states of singly occupied $T_2$ or E and the ground state (called "donor excitation energy $A_1$-$T_2$(E)" in the Table 1) corresponds to the valley-orbit splittings of donor states in bulk Si. The vertical value is calculated at the same geometry (the ground state geometry). The adiabatic value is calculated at the individually optimized geometries. The vertical donor excitation energies $A_1$-$T_2$ for P, As and Sb doped nanocrystals are 0.48, 0.57, and 0.37 eV, respectively. The trend is consistent with the corresponding experimental bulk values:[24] 0.012, 0.021, and 0.010 eV.

Just as in the bulk, the order of the donor state energies follows the weight of the orbital near the donor atom. As shown in Figure 3, the $A_1$ orbital has a large projection on the central dopant atom with s-like symmetry. The $T_2$ orbitals have less weight and p-like symmetry and the E orbitals have the least weight. Therefore, the dopant atom in the center stabilizes the $A_1$ state more than the $T_2$ and E states. Figure 1 compares this $A_1$ orbital in the undoped parent anion to the P doped crystallite. Although the tetrahedral lobe structure is similar, the P dopant causes significant contraction of the orbital with

large density on the P-Si bonds. The central portion of the $A_1$ state is very similar for the smaller $Si_{34}PH_{36}$ and the $Si_{86}PH_{76}$ nanocrystals. In contrast, the $T_2$ (E) orbital of the $Si_{86}PH_{76}$ excited state with $T_2$ (E) singly occupation is the same as the corresponding orbital of the $Si_{87}H_{76}$ anion excited state.

In Table 1, the ionization and affinity energies for the P, As, and Sb-doped nanocrystal are compared to those of the parent. Relative to the undoped parent, the ionization potential is reduced by about 3 eV in each case while the electron affinity is increased by about 0.4 eV. The electron and hole reorganization energies are similar in magnitude to the parent. For the $T_2$ and E excited states, the Jahn-Teller relaxation is about 0.15 eV. This relatively large relaxation energy is often seen for deep level defects in bulk semiconductors, but not for shallow impurities like P. The chemical potential is shifted up by 1.2-1.3 eV, consistent with electron doping, while the hardness is reduced substantially. The effective charging energy drops to about 2 eV. An effective donor binding energy is defined by the difference between the ionization energy of the doped nanocrystal $Si_{86}XH_{76}$ and the electron affinity of the undoped nanocrystal $Si_{87}H_{76}$, corresponding to:

$$Si_{86}XH_{76}^{\ 0} + Si_{87}H_{76}^{\ 0} \rightarrow Si_{86}XH_{76}^{\ +} + Si_{87}H_{76}^{\ -} \qquad (1)$$

First, the doped dot is ionized; i.e., the electron is physically removed from the nanocrystal. Then it is added to a dot of equivalent size without an impurity atom being present. This definition of electron binding energy for the donor in a nanocrystal is equivalent to the usual bulk definition. A similar approach was used in the literature[13,25]. Our calculated donor binding energies for P, As and Sb-doped $Si_{87}H_{76}$ are 2.38, 2.42 and 2.29 eV, respectively. The trend is in agreement with the experimental bulk binding

energies[24], which are 0.046, 0.054, 0.043 eV, respectively. The trend is also consistent with the energies of the singly occupied $A_1$ orbital as shown in Figure 2. The N case is again different, showing large reorganization energies and a chemical potential similar to the parent nanocrystal.

In $Si_{34}PH_{36}$ the vertical (adiabatic) ionization potential is 4.07 (3.83) eV; in $Si_{86}PH_{76}$ it is 3.95 (3.84) eV (6-31g* basis set). Our results for center doped $Si_{86}PH_{76}$ agree well with those of Melnikov and Chelikowsky[13]. Using different DFT methods they report the vertical ionization potential is 4.2 eV. Although the ionization potential changes by a small amount with size, the $|\Psi(0)|^2$ for the $A_1$ orbital systematically drops. The hyperfine splitting in the electron spin resonance is proportional to the orbital weight on the P nucleus. In the present calculation, the predicted ratio of hyperfine splitting between $Si_{34}PH_{36}$ and $Si_{86}PH_{76}$ is 1.28, which is consistent with Melnikov and Chelikowsky[13].

**B. Acceptors**

The optimized structure for center B doping has a nearest neighbor B-Si bond contraction, to 2.12 Å from 2.38 Å Si-Si bond in the parent nanocrystals, and a symmetry lowering to $D_2$. The shortened bonds also occur in substitutional B doping of bulk Si, with very similar magnitude[26]. There is only a very slight change in structure for the positive and negative ions. The local bonding remains $sp^3$. In $Si_{86}AlH_{76}$, $Si_{86}GaH_{76}$, and $Si_{86}InH_{76}$, the four central X-Si bond lengths are 2.47 Å, 2.46 Å and 2.58 Å, respectively. If an extra electron is added (removed), the reoptimized bond length shortens (lengthens) slightly by 0.03 Å.

The electronic energy levels for the acceptor-doped nanocrystals are compared to the parent in the Figure 2. The lowered symmetry splits the three-fold degenerate parent $T_2$ HOMO states into $B_1$, $B_2$ and $B_3$ states. The highest singly occupied $B_1$ states are shifted into the parent HOMO-LUMO gap by 0.2-0.5 eV. The drop in symmetry from $T_d$ to $D_2$ is only nominal in these cases. The doubly occupied $B_2$ and $B_3$ orbitals are only split from the $B_1$ state by about 0.02 eV. Figure 1 shows the singly occupied $B_1$ orbital is essential same as the highest singly occupied orbital of parent cation.

The calculated ionization potential and electron affinity energies are summarized in Table 2. Relative to the parent nanocrystal, the ionization potential is reduced by 0.2-0.5 eV while the electron affinity is substantially increased by about 3 eV. The reorganization energies show more chemical dependence with the Ga and In cases being noticeably larger then the parent undoped nanocrystal. The chemical potential is deeper by 1.1-1.5 eV, consistent with hole-doping. The chemical hardness is much smaller, about 2 eV, which is similar to the donor case.

Similarly to the donor binding energy, we define the acceptor binding energy as the difference between the ionization energy of the undoped nanocrystal and the electron affinity of the hole doped nanocrystal. As shown in the Table 2, the acceptor binding energies for B, Al, Ga, and In-doped $Si_{87}$ are 2.13, 2.34, 2.38, and 2.55 eV, respectively. This trend with acceptor is consistent with the corresponding experimental bulk values[24]: 0.045, 0.069, 0.071, 0.155 eV. The absolute values of the changes with acceptor species are larger, but the relative impact is much smaller than in the bulk. This trend also agrees with the acceptor energy levels of singly occupied orbitals as shown in Figure 2. Finally, we note that the change in the vertical (adiabatic) electron affinity for the B doped

crystallites with size is relatively small: 4.58 (4.66) eV for $Si_{86}BH_{76}$ versus 4.30 (4.57) eV for $Si_{34}BH_{36}$.

## IV. Discussion

The understanding of electronic states of shallow donors and acceptors in bulk semiconductor starts from the hydrogenic model: an extra electron or hole attracted to the ionized donor or acceptor by a statically screened Coulomb attraction $e^2/\varepsilon r$, moving with effective mass m*. This picture can be refined to include anisotropic band mass, multiple valleys (donors in silicon), multiple bands (light and heavy holes) and incomplete screening at short range[12]. The chemical trends highlight the importance of the dopant potential near the dopant atom caused both by differences in the dopant core region as well as differences in local bond lengths. For a doped nanocrystal, all of these factors change: the local bond lengths may differ, the extra hole or electron wavefunction is strongly influenced by the surface of the crystallite and the screening of the Coulomb interaction may be altered. Indeed, for the smaller nanocrystals, the notion of using a continuum dielectric model has been seriously questioned[25,27]. Based on the ab initio calculations, some of these issues can be addressed.

For a strong perturbation, such as the region near an impurity, the screening response need not even be linear. However, with the full self-consistent calculations, we can define an effective impurity potential, one with which the extra electron or hole associated with the impurity interacts. For example, for the P donor case we consider the difference of electrostatic potential (ESP) between the $Si_{86}PH_{76}$ cation and the $Si_{87}H_{76}$ neutral (at the $Si_{86}PH_{76}$ geometry):

$$\Delta V_{Donor} = V_{ESP}(Si_{86}PH_{76}^{+}) - V_{ESP}(Si_{87}H_{76}^{0}) \quad (2)$$

This isolates the screening response of all of the other electrons to the change from Si to P at the center of the nanocrystal. The potential so calculated is the analogue of the usual screened Coulomb potential, but taking into account the local fields and non-linearities in the screening. This has been calculated on a cubic grid points in real space from the Jaguar program[18] and averaged to give a radial, effective potential energy. This is shown in Figure 4a for three examples: donors P and As and the acceptor Al. Several features are evident. First, the effective potential energy is essentially the same outside a radius of 3 Å for all three cases. Second, there are substantial differences inside 2 Å. The polarization of the four inner bonds connected to the impurity atom is quite different among the impurity atoms consistent with their different Pauling electronegativity values[28] i.e. Si (1.8), P (2.1), Al (1.5) and As (2.0). Third, we note that the P case, with a larger electronegativity, shows more screening than the As case. The effective potential energy is smaller in the region out to 2 Å. Fourth, the Al acceptor case, shown here with a choice of sign that corresponds to binding of a hole, is remarkably similar to the P case. This is consistent with the difference in electronegativity being the same magnitude (0.3), but different in sign.

The effective impurity potential illustrated in Figure 4a can be compared to the dielectric screening model in two ways. First, the model of a spherical, uniform dielectric medium with a point charge at the center predicts[8,25]:

$$V_{\mathrm{mod}\,el}(r) = \begin{cases} -\frac{e^2}{e_{eff}\,r} - \left(1 - \frac{1}{e_{eff}}\right)\frac{e^2}{R}, (r \le R) \\ -\frac{e^2}{r}, (r > R) \end{cases} \quad (3)$$

In Eq. (3), $r$ is the distance from the nanocrystal center, $R$ is the radius of the nanocrystal, $e_{eff}$ is the effective dielectric constant of the nanocrystal, and $e$ is the electron charge. This model potential is compared to the effective impurity potentials in Figure 4a, using a radius of 8 Å for $Si_{86}XH_{76}$ and an effective dielectric constant of 6. The agreement between this empirical model and the full quantum mechanical calculation is very good for r greater than 4 Å. The value of the effective dielectric constant entering the model is quite close to the empirical value proposed by Lannoo et al[25] for use with nanocrystals of 8 Å radius. In the short range, there are substantial deviations from the uniform dielectric medium model. These deviations, which depend on the impurity, correspond to the central cell effect in the literature on shallow impurities in bulk semiconductors. A second way to represent the screening of the impurity potential is to define an effective position-dependent dielectric constant through the equation

$$V_{impurity}(r) = -\frac{e^2}{\tilde{e}(r)r} \qquad (4)$$

where the $V_{impurity}(r)$ is the effective impurity potential, as in Figure 4a. This is equivalent to the analysis used by Ogut et al[27] to represent their quantum mechanical calculation of the linear response dielectric screening in silicon nanocrystals. The results for the position dependent dielectric constant are shown in Figure 4b. For comparison to Ogut et al[27], the results for the $Si_{34}PH_{36}$ doped cluster are also plotted. The overall shape is similar to their linear response results. However, the peak value is larger and occurs at smaller radius. This is due to a combination of the polarization in the Si-P bond and non-linearities in the response. The results in Figure 4b for the $Si_{87}$ based nanocrystals are consistent with the observations above. Outside a radius of 3 Å, the screening is

independent of the chemical details of the impurity. Inside 2 Å, the variations with impurity are large and consistent with electronegativity differences.

Based on the qualitative features in Figure 4, we can analyze the physical effects that lead to the large donor and acceptor binding energies in Si nanocrystals. The most significant effect is the reduced screening of the impurity potential. As seen in Figure 4b, the screening inside the nanocrystal is much less effective than long range screening in bulk Si ($\varepsilon$=11.4). As a base line, Figure 4a suggests that the uniform dielectric medium model describes the impurity potential outside the first neighbor shell. If the confinement of the impurity electron or hole is described by a simple envelope wavefunction (sin($\pi$*r/R)/r), then the estimated binding energy would be $(1+\frac{1.44}{e_{eff}})\frac{e^2}{R}$ [25]. For $Si_{86}XH_{76}$, the binding energy estimated from this model is 2.2 eV, remarkably close to our calculated donor and acceptor binding energies from the all-electron quantum mechanical calculations in Table 1 and 2. The residual contributions to the donor and acceptor binding energies of a few tenths eV are then due to the central cell effects. In the usual terminology, this captures the deviations from the uniform dielectric medium model at short range due to local field effects, chemical differences and bond length changes. The influence of local bond length changes was not included in Figure 4. Valley orbit splittings, the donor $T_2$-$A_1$ and E-$A_1$ splittings, derive from the same short range potentials and have a similar magnitude in our calculations for the Si nanocrystals (about 0.5 eV).

These central cell and valley orbit contributions are substantially larger than in the bulk case. This is not generally surprising because they scale with the donor or acceptor wavefunction at short range. Confinement due to the nanocrystal surface significantly

enhances the relative weight of the wavefunction near the donor and acceptor atom. This has been previously used to explain the hyperfine splittings in the P doped Si nanocrystals[13]. Using a simple envelope wavefunction as a guide once again suggests that the central cell and valley orbit contributions scale as $1/R^3$. For small nanocrystals, this highlights the quantitative significance of these local contributions, although full calculations may suggest a different power law for the scaling.

One of the striking features illustrated in Figure 1 is the strong influence of the donor impurity potential on the $A_1$ donor electron orbital. The HOMO in P-doped nanocrystal (Figure 1b) is much tighter than the corresponding orbital in the undoped anion (Figure 1a). By contrast, the acceptor impurity potential does not show such a contraction of the orbital density; the orbital distribution remains relatively rigid, being determined by the surface of the small nanocrystal. This is also seen in the orbital energies in Figure 2. The donor $A_1$ level is split from the parent LUMO by roughly 1 eV, while the acceptor $B_1$ is only split from the parent $T_2$ HOMO by 0.2 – 0.5 eV, depending on the acceptor. In the understanding of the shallow donors like P in bulk Si, it was early recognized through comparison to electron spin resonance data that the donor wavefunction had much more weight near the P nucleus (by roughly one order of magnitude) than predicted by the Wannier model[29]. The qualitative explanation for this is the combination of the strong impurity potential at short-range (Figure 4a) and the s-like symmetry of the $A_1$ orbital around the impurity site. This significantly distorts the donor wavefunction at short range. By contrast, the acceptor wavefunctions are p-like around the acceptor site and are therefore less sensitive to the short-range part of the potential. The other interesting, related question was whether the donor state was in fact completely

localized on the impurity site. The hyperfine splitting data as a function of nanocrystal radius[13] already answers this question: the donor wavefunction spreads out as the nanocrystal size increases. The very weak size dependence of the ionization potential[13] can be understood when the central cell contribution is explicitly considered. In the rough scaling of the envelope function model, it contributes a term that scales as $-1/R^3$. When this is included in the phenomenological framework of Lannoo et al[25], with our estimates of the magnitude of the central cell correction, the donor ionization potential is constant over the 5-25A radius range to within 5% or so.

## V. Conclusion

A dopant in the center of $Si_{87}H_{76}$ is only three Si-Si bonds away from the nanocrystal surface. The introduced carrier is confined in a volume that is roughly two orders of magnitude smaller than in the bulk hydrogenic Wannier orbital. Furthermore, the screening of the Coulomb interaction is much weaker. Nevertheless, this does not lead to "self-trapping" on the atomic scale. The local geometry around the dopant in all cases is very similar to that of the bulk dopant[30]. The orbital of the confined carrier that we calculate changes smoothly with nanocrystal size and we would expect that it will evolve smoothly into the Wannier orbital as size increases further towards the bulk limit. In doped $Si_{87}H_{76}$ the nanocrystal structure does re-adjust modestly if the extra carrier is removed; the electron and hole reorganization energies are 0.1- 0.2 eV. These vibronic energies create barriers to electron transfer; with these energies, rates could be calculated using standard models[31].

Our results for the full range of group-V donors and group-III acceptors allow us to isolate the local chemical contribution and the role of the screened impurity potential. We find substantially enhanced donor and acceptor binding energies, largely driven by the reduced screening of the impurity potentials. The local chemical effects on the donor and acceptor binding energies are also significantly larger than in the bulk crystal due to the enhanced weight of the donor and acceptor wavefunctions on the impurity atoms. The weak dependence of the ionization potential on size traces to the balance of kinetic energy, screened Coulomb potential and local chemical effects. Finally, the donor and acceptor states have quantitatively different interactions with the impurity potential due to the different atomic character of those states near on the impurity atom. As a consequence, the energy splittings of the donor and acceptor states are substantially different.

## Acknowledgments

We thank J. Bevk, M. Stavola and D.V. Lang for informative discussion and correspondence. This work has been supported by the Department of Energy, Basic Energy Sciences, under DEFG0290ER14162 and DEFG0298ER14861. This work was partially supported by the Nanoscale Science and Engineering Initiative of the National Science Foundation under NSF Award Number CHE-0117752 and by the New York State Office of Science, Technology, and Academic Research (NYSTAR). This work was supported in part by the Columbia MRSEC under DMR0213574.

## References

[1] For reviews of Si nanocrystals see N. Koshida, N. Matsumoto, Materials Science and Eng. R40, 169 (2003); D. Kovalev, H. Heckler, G. Polisski, J. Diener, F. Koch, Optical

Materials 17, 35 (2001); as well as the monograph Light Emission in Silicon: From Physics to Devices, Volume 49 in the series Semiconductors and Semimetals (Academic Press, 1998, D. J. Lockwood, editor).

[2] H. Mizuno, H. Koyama, and N. Koshida, Applied Physics Letters **69** (25), 3779 (1996); M. V. Wolkin, J. Jorne, P. M. Fauchet et al., Physical Review Letters **82** (1), 197 (1999); J. S. Biteen, N. S. Lewis, H. A. Atwater et al., Applied Physics Letters **84** (26), 5389 (2004).

[3] Z. Y. Zhou, R. A. Friesner, and L. Brus, Journal of the American Chemical Society **125** (50), 15599 (2003).

[4] Z. Y. Zhou, L. Brus, and R. Friesner, Nano Letters **3** (2), 163 (2003).

[5] L. T. Canham, Applied Physics Letters **57** (10), 1046 (1990).

[6] L. Brus, J. Phys. Chem. **98**, 3575 (1994).

[7] P. D. J. Calcott, K. J. Nash, L. T. Canham et al., Journal of Physics-Condensed Matter **5** (7), L91 (1993); M. S. Hybertsen, Physical Review Letters **72** (10), 1514 (1994).

[8] L. E. Brus, Journal of Chemical Physics **79** (11), 5566 (1983).

[9] G. Allan, C. Delerue, M. Lannoo et al., Physical Review B **52** (16), 11982 (1995).

[10] L. Brus, Physical Review B **53** (8), 4649 (1996).

[11] B. E. Kane, Nature **393** (6681), 133 (1998); A. S. Martins, R. B. Capaz, and B. Koiller, Physical Review B **69** (8), 085320 (2004); L. M. Kettle, H. S. Goan, S. C. Smith et al., Physical Review B **68** (7), 075317 (2003).

[12] W. Kohn and J.M. Luttinger, Phys. Rev. **98**, 915 (1955); A. Baldereschi, Phys. Rev. B **1**, 4673 (1970); J.C. Phillips, Phys. Rev. B **1** (4), 1540 (1970); N. Binggeli and A. Baldereschi, Physical Review B **45** (11), 5944 (1992).

[13] D. V. Melnikov and J. R. Chelikowsky, Physical Review Letters **92** (4), 046802 (2004).

[14] A. D. Becke, Journal of Chemical Physics **98** (7), 5648 (1993).

[15] K. Raghavachari, Theoretical Chemistry Accounts **103** (3-4), 361 (2000).

[16] J. Muscat, A. Wander, and N. M. Harrison, Chemical Physics Letters **342** (3-4), 397 (2001).

[17] J. K. Perry, J. Tahir-Kheli, and W. A. Goddard, Physical Review B **65** (14), 144501 (2002); K. N. Kudin, G. E. Scuseria, and R. L. Martin, Physical Review Letters **89** (26), 266402 (2002); X. B. Feng and N. M. Harrison, Physical Review B **69** (13), 132502 (2004); D. Munoz, N. M. Harrison, and F. Illas, Physical Review B **69** (8), 085115 (2004).

[18] Jaguar 5.0, Schrodinger, L.L.C., Portland, OR, 1991-2003.

[19] W.R. Wadt and P.J. Hay, J. Chem. Phys. **82**, 284 (1985).

[20] C. S. Nichols, C. G. Vandewalle, and S. T. Pantelides, Physical Review B **40** (8), 5484 (1989).

[21] M. Scheffler, Physica B-Condensed Matter **146**, 176 (1987).

[22] M. Saito and Y. Miyamoto, Physical Review B **56** (15), 9193 (1997).

[23] B. Delley and E. F. Steigmeier, Physical Review B **47** (3), 1397 (1993); S. Y. Ren, Physical Review B **55** (7), 4665 (1997); F. A. Reboredo, A. Franceschetti, and A. Zunger, Physical Review B **61** (19), 13073 (2000); Y. M. Niquet, C. Delerue, G. Allan et al., Physical Review B **62** (8), 5109 (2000).

[24] Zahlenwerte und Funktionen aus Naturwissenschaften und Technik, in Vol. III of Landolt-Bornstein (Springer, New York, 1982), pt. 17a.

[25] M. Lannoo, C. Delerue, and G. Allan, Physical Review Letters **74** (17), 3415 (1995).

[26] J. Zhu, T. D. delaRubia, L. H. Yang et al., Physical Review B **54** (7), 4741 (1996).

[27] S. Ogut, R. Burdick, Y. Saad et al., Physical Review Letters **90** (12), 127401 (2003).

[28] Linus Pauling, *The Nature of the Chemical Bond*, 3rd ed. (Cornell University Press, Ithaca, 1960).

[29] W. Kohn and J.M. Luttinger, Phys. Rev. **97**, 883 (1955); W. Kohn, in *Solid State Physics*, edited by F. Seitz and D. Turnbull (Academic, New York, 1957), Vol. 5, pp. 257.

[30] In separate calculations, we have found that if the dopant is closer to the surface, or if the surface has polar Si-O bonds, then dopant structure can change. (to be published).

[31] B.K. Ridley, *Quantum Processes in Semiconductors*, 2nd ed. (Oxford Press, London, 1988); R. A. Marcus and Norman Sutin, Biochimica et Biophysica Acta **811** (3), 265 (1985).

**Table 1. Properties of structurally optimized group-V element doped Si86XH76. All energies are in eV.**

| Species | $Si_{86}NH_{76}$ | $Si_{86}PH_{76}$ | $Si_{86}AsH_{76}$ | $Si_{86}SbH_{76}$ | $Si_{87}H_{76}$ |
|---|---|---|---|---|---|
| Symmetry of neutral species | C3v | Td | Td | Td | Td |
| donor excitation A1-T2(vertical) | | 0.48 | 0.57 | 0.37 | |
| donor excitation A1-T2(adiabatic) | | 0.3 | 0.42 | 0.23 | |
| donor excitation A1-E(vertical) | | 0.59 | 0.7 | 0.57 | |
| donor excitation A1-E(adiabatic) | | 0.44 | 0.51 | 0.43 | |
| Adiabatic Ionization Potential $\mathbf{I_a}$ | 4.98 | 3.84 | 3.88 | 3.75 | 6.79 |
| Vertical Ionization Potential $\mathbf{I_v}$ | 5.68 | 3.95 | 3.99 | 3.86 | 6.87 |
| Hole Reorganization Energy $\mathbf{?_h}$ | 0.7 | 0.1 | 0.11 | 0.11 | 0.08 |
| Adiabatic Electron Affinity $\mathbf{EA_a}$ | 3.11 | 1.87 | 1.92 | 1.84 | 1.46 |
| Vertical Electron Affinity $\mathbf{EA_v}$ | 2.72 | 1.79 | 1.83 | 1.76 | 1.43 |
| Electron Reorganization Energy $\mathbf{?_e}$ | 0.39 | 0.08 | 0.09 | 0.09 | 0.04 |
| Donor Binding Energy $\mathbf{E_b}$ | 3.52 | 2.38 | 2.42 | 2.29 | |
| Adiabatic Chemical Potential m | -4.04 | -2.86 | -2.9 | -2.8 | -4.12 |
| Adiabatic Chemical Hardness h | 1.87 | 1.97 | 1.96 | 1.91 | 5.33 |

**Table 2. Properties of structurally optimized group-III element doped Si86XH76.**

**All energies are in eV.**

| Species | $Si_{86}BH_{76}$ | $Si_{86}AlH_{76}$ | $Si_{86}GaH_{76}$ | $Si_{86}InH_{76}$ | $Si_{87}H_{76}$ |
|---|---|---|---|---|---|
| Symmetry of neutral species | D2 | D2 | D2 | D2 | Td |
| Adiabatic Ionization Potential $\mathbf{I_a}$ | 6.56 | 6.39 | 6.39 | 6.24 | 6.79 |
| Vertical Ionization Potential $\mathbf{I_v}$ | 6.66 | 6.47 | 6.53 | 6.40 | 6.87 |
| Hole Reorganization Energy $\mathbf{?_h}$ | 0.10 | 0.09 | 0.14 | 0.16 | 0.08 |
| Adiabatic Electron Affinity $\mathbf{EA_a}$ | 4.66 | 4.45 | 4.40 | 4.24 | 1.46 |
| Vertical Electron Affinity $\mathbf{EA_v}$ | 4.58 | 4.28 | 4.22 | 4.06 | 1.43 |
| Electron Reorganization Energy $\mathbf{?_e}$ | 0.07 | 0.17 | 0.18 | 0.18 | 0.04 |
| Acceptor Binding Energy $\mathbf{E_b}$ | 2.13 | 2.34 | 2.38 | 2.55 | |
| adiabatic Chemical Potential m | -5.61 | -5.42 | -5.40 | -5.24 | -4.12 |
| adiabatic Chemical Hardness h | 1.90 | 1.94 | 1.99 | 1.99 | 5.33 |

**Figure 1. (Color online) HOMO isosurface plots of 6 hydrogen-passivated species: (a) Si35H36 anion, (b) Si34PH36 neutral, (c) Si87H76 anion, (d) Si86PH76 neutral, (e) Si87H76 cation, (f) Si86BH76 neutral.**

(a) Si35H36-

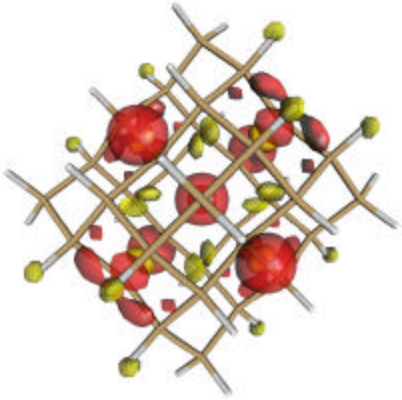

(b) Si34PH36

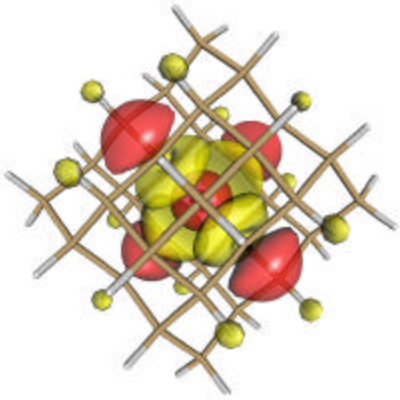

(c) Si87H76-

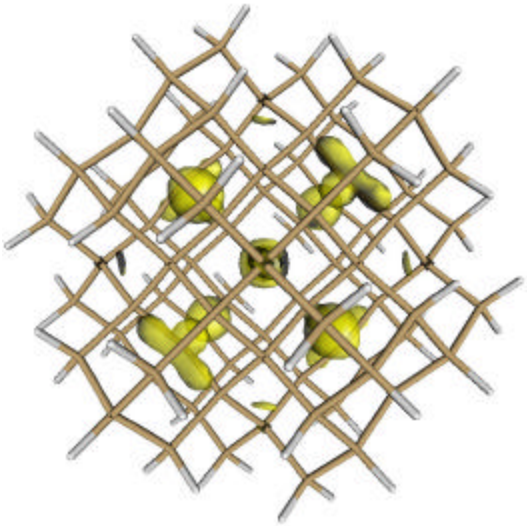

(d) Si86PH76

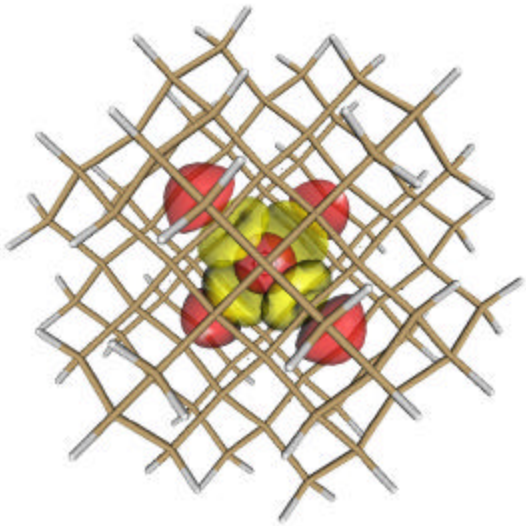

(e) Si87H76+

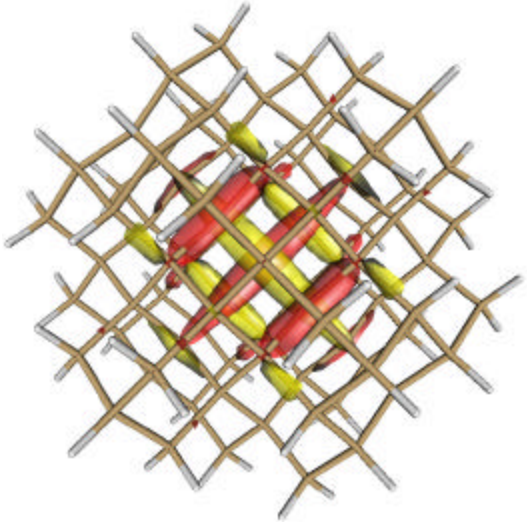

(f) Si86BH76

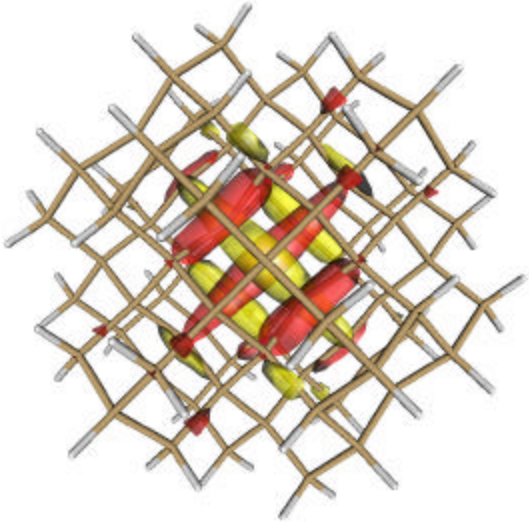

**Figure 2. (Color online) Electronic energy levels near the HOMO and LUMO for the doped Si86XH76 and undoped Si87H76 Si nanocrystals. Key energy levels are labeled according to symmetry and the dots indicate occupancy of the HOMO. The long dashed lines indicate the HOMO and LUMO energies of the parent undoped nanocrystal.**

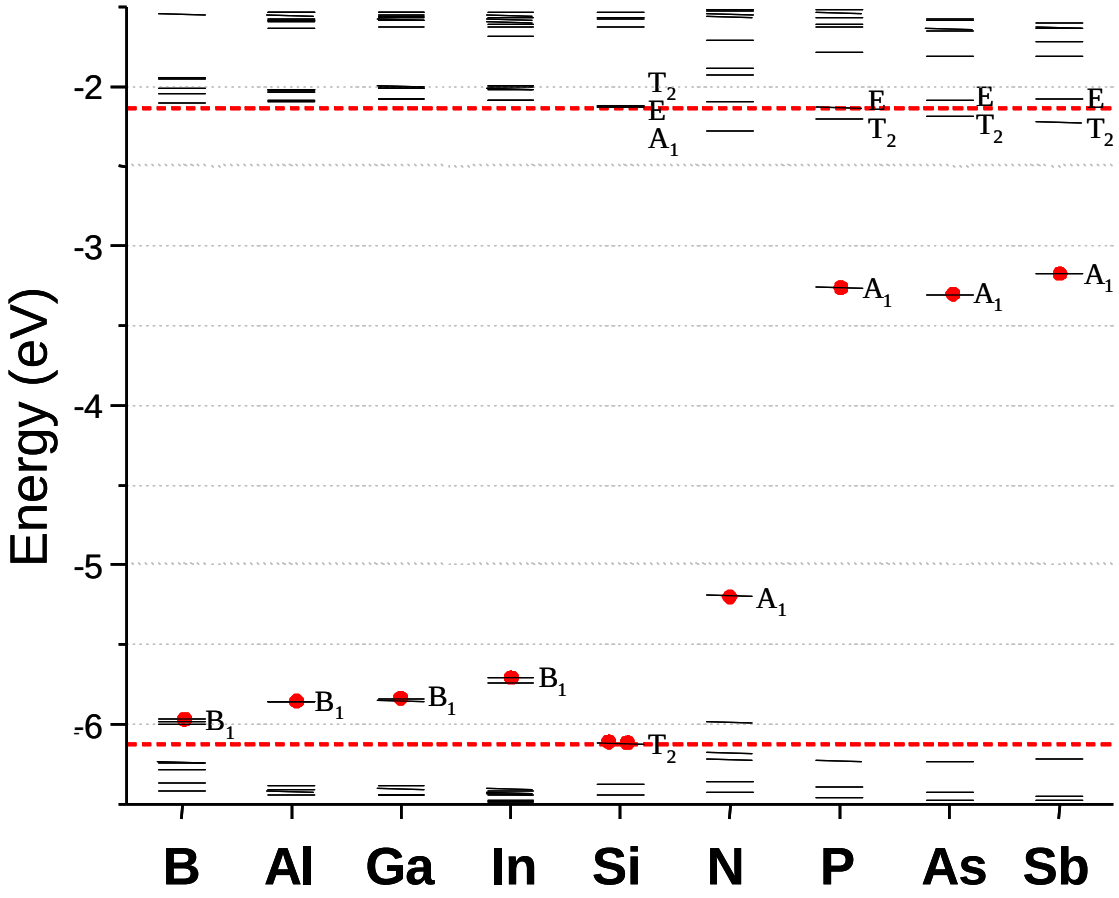

**Figure 3. (Color online) Isosurface plots (a), (b), (c) and line plots (d), (e), (f) for the three symmetry distinct P impurity states of Si86PH76. In (d), the whole range of wavefunction near center is not shown.**

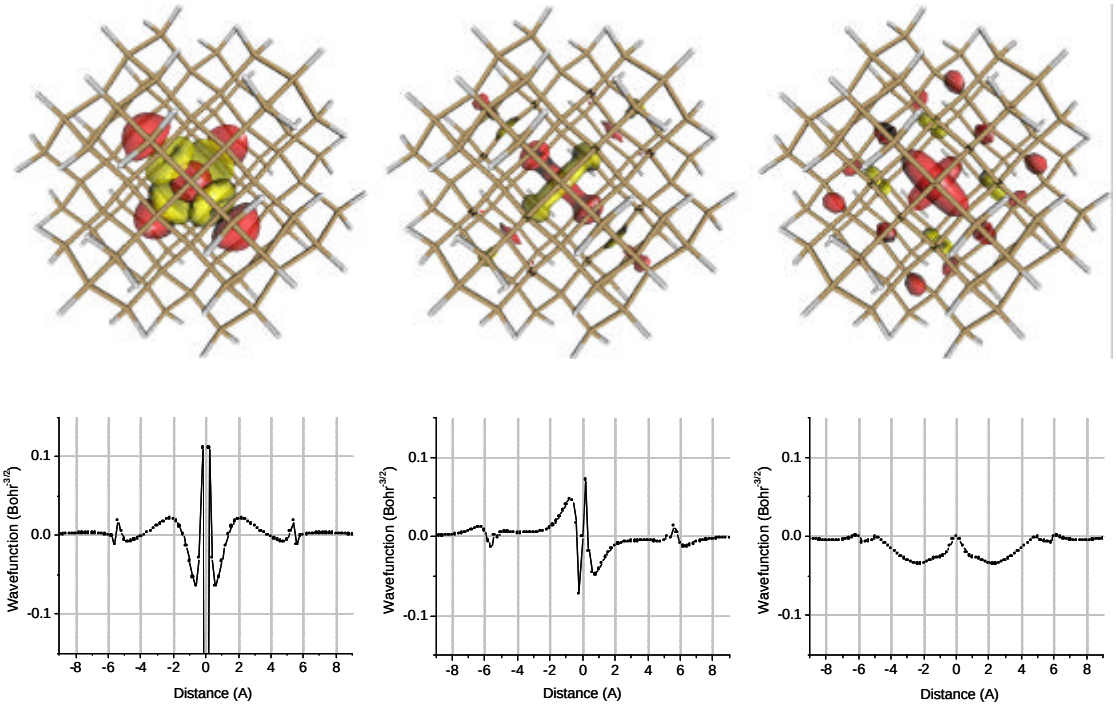

**Figure 4. (Color online) (a) Effective impurity potential for the doped nanocrystals Si86XH76.together with a model potential as described in the text. (b) Effective radially dependent dielectric constant for each doped nanocrystal as defined in the text. Lines are guides through the data points.**